Scanning Probe Microscopy Studies of Solid-State Molecular Electroluminescent Devices Based on Tris(2,2′-bipyridine) Ruthenium(II) Complexes

Fu-Ren F. Fan and Allen J. Bard*

Department of Chemistry and Biochemistry, The University of Texas at Austin, Austin, Texas 78712

Received: September 27, 2002; In Final Form: December 3, 2002

The charge injection, transport, and light emission of a solid-state molecular electrochemiluminescent thin (100 nm) film of tris(2,2′-bipyridine) ruthenium(II) complex, $Ru(bpy)_3(ClO_4)_2$, was investigated with tuning-fork-based scanning probe microscopy (TFSPM) in combination with electroluminescence and current measurements as a function of potential. Spin-cast $[Ru(bpy)_3(ClO_4)_2]$ thin films are shown to contain rather uniformly distributed nanostructures. These nanostructures produce heterogeneity in the current and luminescence responses of the films. Both single and double charge carrier (unipolar and bipolar) injection can take place in these thin films, depending on the magnitude of the bias voltage. Potential-step transients allow the determination of the effective diffusion coefficients of charge carriers. The effective diffusion coefficients of electrons or holes depend strongly on the electric field strength (or the applied voltage). We have also used the TFSPM to penetrate the $[Ru(bpy)_3(ClO_4)_2]$ thin film to estimate the local thickness of the film.

I. Introduction

With growing interest in solid-state molecular electroluminescent devices (MELDs) (sometimes generically called "organic" light emitting devices or OLEDs), efforts have been made to investigate such devices based on thin films of polymers or small molecules.[1] The ruthenium(II) complexes of bipyridine, phenanthroline, and their derivatives that have been extensively studied in electrogenerated chemiluminescence (ECL) in solution have recently been used in solid-state-based light-emitting devices.[2] High-brightness and high-efficiency emissions with short delay times to reach maximum emission have been reported.[3] However, the emission in these cells decreases with time. The origin of this decay is currently under investigation and appears to be related to the generation of a quencher from the excited state of $Ru(bpy)_3^{2+}$. Rudmann et al.[2h] suggest that when the cell is operated under low voltage conditions, the light output is more stable. An electrochemical mechanism has been suggested as operative in these solid-state devices, as originally proposed in solution phase ECL.[4,5] In these devices, current flow occurs by electron injection into a bipyridine ligand at the negatively biased electrode and hole injection into the Ru(II) center at the positively biased electrode. In the bulk of thin film, electric-field-driven charge hopping between electronically localized redox sites occurs until a radiative or nonradiative recombination takes place.

In previous publications,[6] we demonstrated that scanning electrochemical microscopy (SECM) provides valuable information about charge transport and thermodynamic parameters. We applied the SECM in combination with chronoamperometry and voltammetry to study the oxidation/reduction behavior of redox polymer or ionically conductive polymer thin films incorporating a redox moiety. An important parameter that depends on the polymer oxidation state is the effective conductance at a given point in a thin film. This represents the combined effects of the electron transport rate to or from a point by electron or hole hopping between oxidized and reduced centers and the ion relaxation that compensates local charge imbalances produced by electron-transfer reactions.

In this work, we utilize tuning-fork-based scanning probe microscopy (TFSPM) in combination with electrogenerated luminescence and other electrochemical techniques to characterize a MELD based on a $[Ru(bpy)_3(ClO_4)_2]$ thin film to obtain a better understanding of the mechanism involved in the charge carrier injection and transport processes in this thin film. We show that spin-cast $[Ru(bpy)_3(ClO_4)_2]$ thin films are not crystalline but rather contain uniformly distributed nanostructures. Our results demonstrate that both single and double charge carrier injection takes place in this thin film, depending on the magnitude of the bias voltage and the time domain of the experiment. The effective diffusion coefficient of electron or hole is also shown to depend strongly on the electric field strength (or the applied voltage).

II. Experimental Section

1. Chemicals. Commercially available $Ru(bpy)_3Cl_2$ (Alfa Products) was converted to $Ru(bpy)_3(ClO_4)_2$ by a metathesis reaction with an excess of $NaClO_4$.[4] The precipitate was washed thoroughly with water to remove excess $NaClO_4$ and dried in a vacuum. All solvents were spectrophotometric grade and were used as received.

2. Film Preparation. Thin films of $Ru(bpy)_3(ClO_4)_2$ were spin cast onto Au (∼20 nm on glass) or indium tin oxide (ITO) substrates (Delta Technologies, Inc., Stillwater, MN) from a 4% (w/v) acetonitrile solution at room temperature with a photoresist spinner (Headway Research Inc., Garland, TX). All films were heated in a vacuum oven at 125 °C for 8 h and then stored in dry argon in the dark at room temperature before the measurements were made.

3. Instrumentation and Methods. The home-built TFSPM used in this experiment was developed from an instrument described previously[7] by incorporating a tuning-fork-based scanning probe microscope (SPM) tip assembly. A sharpened
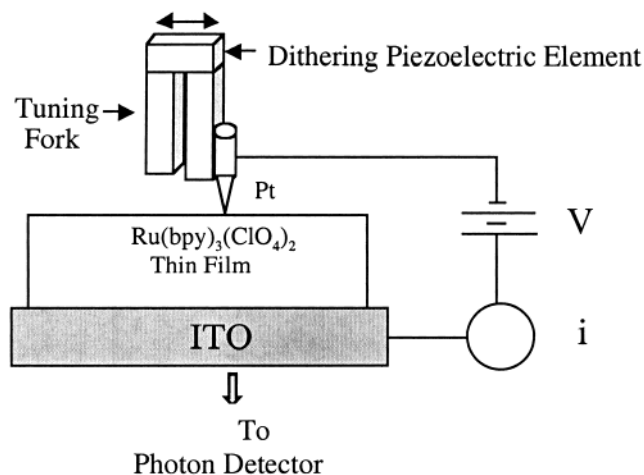
1782 *J. Phys. Chem. B, Vol. 107, No. 8, 2003*

Fan and Bard

Figure 1. Schematic representation of the measurement with a tuning-fork-based SPM tip contacting the surface of a $Ru(bpy)_3(ClO_4)_2$ thin film on ITO substrate.

Pt wire (diameter $\sim100~\mu$m) serving as the tip was glued along the side of one of the prongs of a quartz crystal tuning fork. Such tuning forks are commercially available for operation at 32768 Hz (Digi-Key, Thief River Falls, MN) or at ca. 90 kHz (ThermoMicroscope, Sunnyvale, CA). The mechanical resonance of the fork was excited with a piezoelectric tube serving to dither the tuning fork so that the tip was vibrated parallel to the sample surface. The construction and testing of this shear force sensor followed closely the procedures reported previously by Karrai and Grober.[8]

Current−voltage responses of $Ru(bpy)_3(ClO_4)_2$ thin films on ITO were examined by voltage steps and sweeps across the ITO substrate and the tip (Figure 1). The voltage was supplied from an EG&G model 175 universal programmer, controlled by an IBM PC equipped with a DT2821 interface board. The pA-level currents were monitored with a high sensitivity current amplifier. The luminescence intensity was measured with a Hamamatsu R4220 photomultiplier tube (PMT) operated at −750 V or a time-resolved photon counting system (model T914P, EG&G). The PMT current was measured with a Keithley model 6517 electrometer.

Specific experimental procedures and parameters will be described in more detail in the individual sections. All measurements were carried out in dry argon if not otherwise mentioned.

III. Results

A film thickness of about 100 nm was determined by making a light scratch on the surface and measuring the line profile across it with an atomic force microscope.[3a] It was also estimated from the difference between the onset substrate displacement to observe current (or shear-force change) and the displacement where tunneling (or abrupt change in the shear force) takes place (Figure 2). See also the next section for a more detailed description about the current (or shear-force change) vs distance relations. The thickness determined from these two techniques agreed reasonably well.

1. Current−Voltage and Luminescence−Voltage Measurements. Figure 3a shows some typical current−voltage and luminescence−voltage plots of a 100 nm thick $Ru(bpy)_3(ClO_4)_2$ layer on ITO with a Pt tip positioned inside the film (about 50 nm deep). As the tip voltage (E_a) was scanned negative with respect to the ITO substrate, significant current began to flow through the device at ca. −1.7 V, while detectable light emission was observed only at tip voltages negative of ca. −2.7 V. Notice
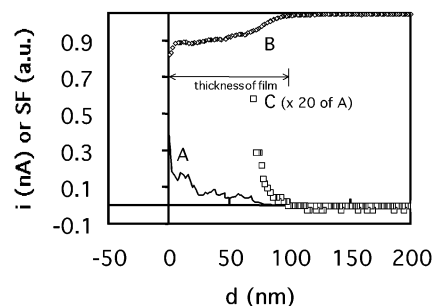

Figure 2. Film thickness measurement from the (current vs distance) (A) or the (shear force vs distance) (B) curves. C is the expanded (20 times) curve of A. Tip was biased at −3.0 V during approach and the tip current is inverted.
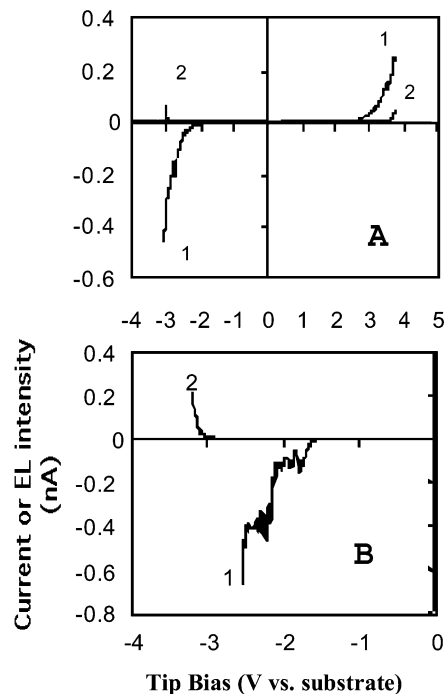

Figure 3. (A) Typical current−voltage (curve 1) and luminescence−voltage (curve 2) plots of a 100 nm thick $Ru(bpy)_3(ClO_4)_2$ layer on ITO with a Pt tip positioned inside the film (ca. 60 nm away from the ITO surface). Voltage scan rate, 0.1 V/s. (B) Several distinct current steps or shoulders were sometimes observed in the negative tip bias region in a different experiment.

that several current steps or shoulders, similar to those observed in voltammograms at microelectrodes in an acetonitrile solution containing $Ru(bpy)_3^{2+}$, were sometimes observed at negative E_a (for example, see Figure 3b), depending on the voltage scan rate. Peak-shaped voltammograms at microelectrodes usually indicate that the potential sweep rate employed is not slow enough to completely establish a steady-state condition.[9] In the positive-bias region, current flow started at ca. +2.3 V, while luminescence was observed at tip bias positive of ca. +2.7 V. These onset voltages for light emission of 2.7 V are slightly higher than those reported for solution ECL of the same compound but are roughly the same as those seen in solid-state devices with different contact materials. Similar voltammetric− and luminescence−voltage behavior was also observed when Au on glass, instead of ITO, was used as the substrate. Detailed results on the effect of the contact materials will be reported elsewhere.

2. Current−Distance, Luminescence−Distance, and Shear Force−Distance Relations. When the tip was biased at +3.0 or −3.0 V with respect to the ITO substrate and it approached

Solid-State Molecular Electroluminescent Devices
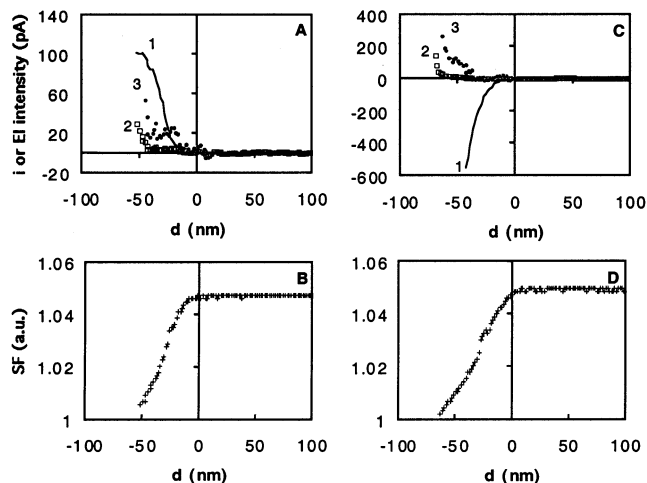
J. Phys. Chem. B, Vol. 107, No. 8, 2003 **1783**

Figure 4. Current, luminescence, and shear force (SF) as functions of distance (d). In frames A and B, tip was biased at +3.0 V, while in frames C and D, tip was biased at −3.0 V. Curves 1 and 2 represented current (i) and luminescence intensity (El), respectively. Curve 3 is the expanded (5 times for frame A and 10 times for frame C) curve of 2.
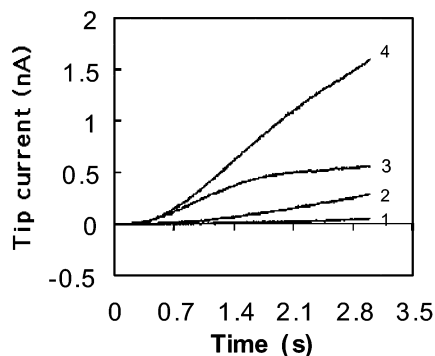

Figure 5. A series of current transients through a ca. 100 nm thick Ru(bpy)$_3$(ClO$_4$)$_2$ layer on ITO as the Pt tip was positioned within the film at ca. 60 nm away from the ITO surface, and a voltage step was applied between tip and substrate. Tip voltage steps: (1) + 2.8 V; (2) + 3.5 V; (3) + 4.0 V; (4) + 4.5 V.

the surface of a Ru(bpy)$_3$(ClO$_4$)$_2$ film, current flow was observed at the position where change in shear force was detected (Figure 4). The current response showed only a slight delay with respect to the shear force response when the tip is biased at +3.0 V. At +3.0 V tip bias, light emission occurred from the surface region of the film as soon as the current flow started through the device. However, at −3.0 V bias, light emission spatially lagged behind both the current and the change in shear force. A delay of the emission with respect to the current at negative bias was also observed when Au, instead of ITO, was used as the substrate. This apparent depth profile of light emission may be mainly associated with the time behavior of the carrier injection and transport as described below, since the luminescence profile was coincident better with the current profile in the reverse displacement scan (not shown).

3. Current Transients. Information about charge carrier injection and field-driven charge transport through the film can be obtained from potential-step transients. Figure 5 shows a series of time-dependent current flows through a ∼100 nm thick Ru(bpy)$_3$(ClO$_4$)$_2$ film coated on ITO as the Pt tip was positioned at ca. 60 nm away from the ITO surface and a voltage step was applied between tip and substrate. The voltage step produced a fast (≤1 ms) transient current spike (barely distinguishable from the *y*-axis) followed by a slow rise. A smaller current spike
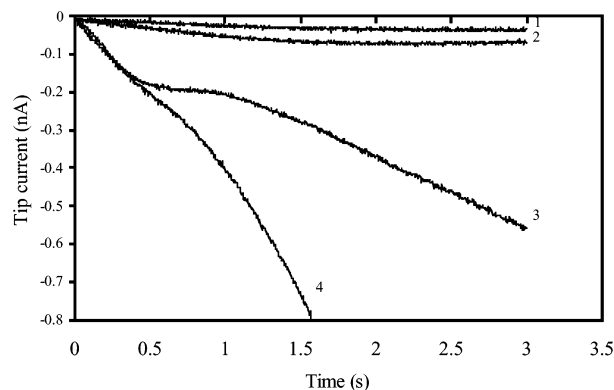

Figure 6. A series of chronoamperometric curves at various negative tip voltage steps: (1) −2.3 V; (2) −2.5 V; (3) − 3.0V; (4) − 3.5 V for same device configuration as used in Figure 5.

was seen when the tip was farther away from the film surface. At least part of the initial current spike is apparently associated with the stray capacitance of the current-measurement circuit, which has a time constant set at ca. 20 μs for this experiment. Part of it is associated with the ionic current of the film, which is discussed below.

As shown in Figure 5, at low positive tip bias (e.g., ≤3.0 V), the current rose slowly and approached a steady-state plateau within a few seconds. An increase of the step voltage to 4.0 V increased the initial rise speed of the current and it reached a steady-state plateau within 2 s. An increase of the step voltage to 4.5 V had no dramatic effect on the shape of the initial part of the current−time curve, but it substantially affected the current on a longer time scale.

Current transients for negative values of E_a were obtained by moving the tip to a nearby location and repositioning the tip again at ca. 60 nm from the ITO substrate. The tip bias was then stepped from 0 V to different negative values, and the current was recorded as a function of time. Four typical curves are shown in Figure 6. For negative E_a positive of −3.0 V, the quasi-steady-state current plateau became larger in magnitude, and the corresponding time to reach the plateau decreased as the potential was made more negative (from curve 1 to curve 3 of Figure 6). When E_a was negative of −3.0 V, the current reached a steady-state plateau within 0.5 s, and then it increased again with time as shown in curves 3 and 4 of Figure 6, suggesting the onset of the second process. Similar behavior was observed when BF$_4^-$, instead of ClO$_4^-$, was the counterion (not shown).

4. Topographic, Current, and Luminescence Images. Information about the morphology, conductance, and luminescence homogeneity of the spin-cast Ru(bpy)$_3$(ClO$_4$)$_2$ films was obtained with TFSPM. Figure 7 shows the topographic and current image at 3.5 V and the luminescence image at −3.5 V of a layer (∼100 nm thick) of Ru(bpy)$_3$(ClO$_4$)$_2$ on ITO, taken simultaneously with a Pt tip. The topographic image was recorded at constant amplitude of shear force, which was set at 2% less than that when the tip was far away from the film surface. The tip bias was pulsed between +3.5 and −3.5 V with pulse duration of a few milliseconds, and the current at +3.5 V and luminescence at −3.5 V tip bias were monitored. In frame A on the left side of Figure 7, we show a micrometer-sized hole as a marker, which was artificially made by a tip crash by approaching the tip to the substrate without turning the feedback loop on. Also shown in frame A on the right side of Figure 7 is a higher resolution image for the portion of surface at the upper left corner of the frame on the left. The image suggests
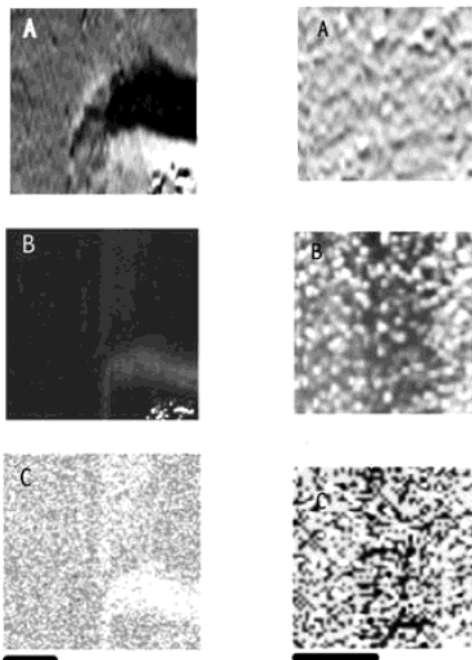
Figure 7. Topographic image (A) and current image at +3.5 V tip bias (B). Luminescence image at −3.5 V (C) of a single layer of Ru-(bpy)$_3$(ClO$_4$)$_2$ on ITO, taken simultaneously with a Pt tip. Tip raster rate is ∼0.25 Hz. Marker is 1 μm.

that the film contains no particularly crystalline grains but rather uniformly distributed nanostructures. Preliminary transmission electron microscope images of these films also suggest that they are amorphous with any crystallites of size <5 nm.[3a] These structures, however, produce heterogeneity in the current and luminescence responses of the film.

IV. Discussion

Ru(bpy)$_3$(ClO$_4$)$_2$ films spin-cast on ITO or Au electrodes exhibit light emission and current flow when a sufficiently high voltage is biased between the substrate and a sharpened Pt tip

positioned inside the films. The topographic image (Figure 7) of a Ru(bpy)$_3$(ClO$_4$)$_2$ thin film shows rather uniformly distributed nanostructures, although pinholes of sub-micrometer dimension are sometimes observed. Current flow and light emission could occur on both positive and negative tip bias. Different shaped voltammograms are observed at negative tip bias (≤ -1.7 V) and positive bias ($\geq +2.3$ V). The situation is quite different for light emission, which occurs at nearly the same voltage of magnitude of ca. 2.7 V for both positive and negative tip voltages. The small difference between the onset voltages for solution and solid-state electrogenerated luminescence could be attributed to different bulk resistance of the film and the electrolyte as discussed below.

1. Charge Carrier Injection. The current flow depends on the sign and magnitude of the tip voltage (with respect to the ITO or Au substrate). At a low negative bias (-2.7 V $< E_a$ < -1.7 V), the initial part of the voltage pulse first causes charging of the tip and ITO. The electric field created across the film then causes ionic movement, in the case here, motion of ClO$_4^-$ away from the tip. This redistribution of charges leads to higher fields near the tip surface. Injection of electrons from the tip (or reduction of Ru(bpy)$_3^{2+}$ at the tip) occurs with electrons moving through the film and injecting into the ITO contact (single carrier or unipolar injection) (Figure 8-I). This unipolar injection process very likely favors the electron transfer occurring at the tip at low bias in the present experimental configuration. Analogous to solution electrochemistry, the current shoulder observed in the negative voltammetric curve (as shown in Figure 3B) probably corresponds to the first reduction wave of Ru(bpy)$_3^{2+}$. From the half-wave bias voltage, we estimate the total voltage drop across the two interfaces and the bulk film for the first reduction to be about 1.8 V. An analogous process with hole-injection (or oxidation of Ru-(bpy)$_3^{2+}$) at the tip occurs with a positive tip bias. At these bias values, the potential drop is not sufficiently high to cause both electron and hole injection into the film.

With single carrier injection, current flows, but no light emission is observed. At higher tip bias values ($|E_a| \geq 2.8$ V),

I. Single Carrier (e.g. electron) injection
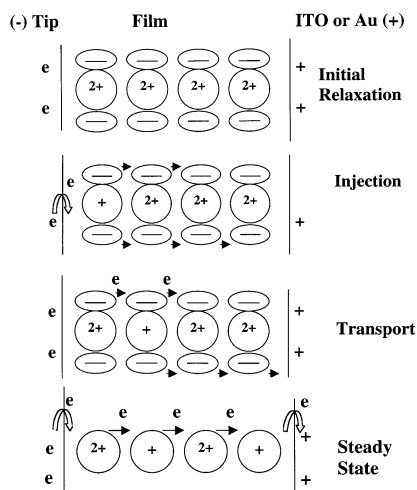
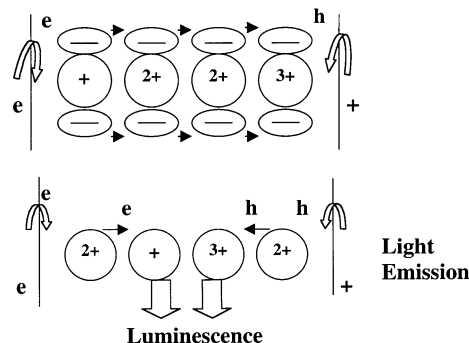## II. Double Carrier (electron and hole) injection

Figure 8. Schematic representation of charge carrier injection and ion redistribution in the film at various stages after application of a voltage step. 2+ represents Ru(bpy)$_3^{2+}$; 3+, Ru(bpy)$_3^{3+}$; $\oplus$, Ru(bpy)$_3^+$; e, electron and h, hole; $\ominus$, for ClO$_4^-$; curved arrows for charge hopping or recombination and straight arrows for ClO$_4^-$ migration, + for positive contact and − for negative contact. (I) Single carrier (e.g. electron) injection. (II) Double carrier (electron and hole) injection.

Solid-State Molecular Electroluminescent Devices

J. Phys. Chem. B, Vol. 107, No. 8, 2003 **1785**

a similar process occurs. However, here, at negative tip bias, both electron injection at the tip and hole injection at the ITO substrate are possible (or vice versa at opposite tip bias). With this double carrier (bipolar) injection, eventual electron-hole annihilation produces an $Ru(bpy)_3^{2+}$ excited state and light emission (Figure 8-II).

2. Charge Carrier Transport. The effective diffusion coefficients of the carriers (D_{eff}) are important in understanding the slow rise in the current after a voltage step is applied to $Ru(bpy)_3^{2+}$-based MELD and why the initiation of light emission lags behind the current flow in the present experimental configuration. We explore the possibility of measuring D_{eff} from the current transients at small voltage steps. Under such conditions, as discussed above, single carrier injection occurs at the tip and no light is emitted. Electron-hole-pair recombination can thus be neglected. We will also consider the electronic current as the diffusion current only and deal with the ionic current (perhaps mainly contributed by anion migration and redistribution inside the film) independently. This simplifies the mathematics, and an approximate analytical solution, eq 1, can be obtained (see eq A13 in the appendix for the derivation).

$$I = I_{e,ss}[erfc(1/(T)^{1/2}) + \{2(1 + 1/L)/(\pi T)^{1/2}\} \exp(-1/T)] + I_{i,0} \exp(-\tau T/\tau_\Omega) \quad (1)$$

where $I = i/i_l$, $I_{e,ss} = i_{e,ss}/i_l$, $I_{i,0} = i_{i,0}/i_l$, $L = \vartheta/r_0$, $T = t/\tau$, $\tau = \vartheta^2/(4D_{eff})$, i_l is the diffusion-limited current plateau, ϑ is the film thickness, r_0 is the radius of curvature of the tip, and the rest of parameters are defined in the Appendix. The first term on the right side of eq 1 is the electronic current, and the second term represents the ionic component. This equation predicts a current−time curve which shows a fast current spike followed by a slowly rising current plateau when the ohmic (charging) or dielectric relaxation time, τ_Ω, is much shorter than τ as observed in most experimental curves. Under such conditions, at long times, the ionic current component is negligible compared to the electronic current component.

Theoretical curves that correspond to experimental curve 3 of Figures 5 and 6 shown in Figure 9 were calculated from (1), with the same values of geometric parameters, $\vartheta = 100$ nm and $L^{-1} = 0.6$ and a small contribution (<5%) from the ionic current, except at the very beginning of the curves. It was possible to fit, quantitatively, those curves obtained at low tip bias, e.g., ≤4.0 V for positive E_a or ≥−3.0 V for negative E_a, when only single carrier injection predominates. It was also possible to fit the initial rising portion of those curves obtained at higher tip bias. On a longer time scale, the fit was not as good, perhaps because other processes, such as double carrier injection or a second reduction of $Ru(bpy)_3^{2+}$, took place. Under such conditions, extensive ion redistribution in the film may also occur, so eq 1 is no longer valid and a refinement of the theory is required. Nevertheless, this simple analytical expression proved sufficiently accurate for the case of low bias to provide a good quantitative fit between the theoretical and experimental results, which allows measuring D_{eff} from the current transients. As shown in Figure 9, a good fit between theory and experiment was obtained for both positive (A) and negative (B) tip bias, when the values of the parameters, e.g., D_{eff}, were adjusted to fit these curves were quite different. As summarized in Figure 10, D_{eff} for both electron and hole are strongly electric-field strength (or voltage bias) dependent, as predicted from the hopping mechanism for carrier transport.[10,11] Thus, large voltage biases can probably be employed to accelerate charge carrier
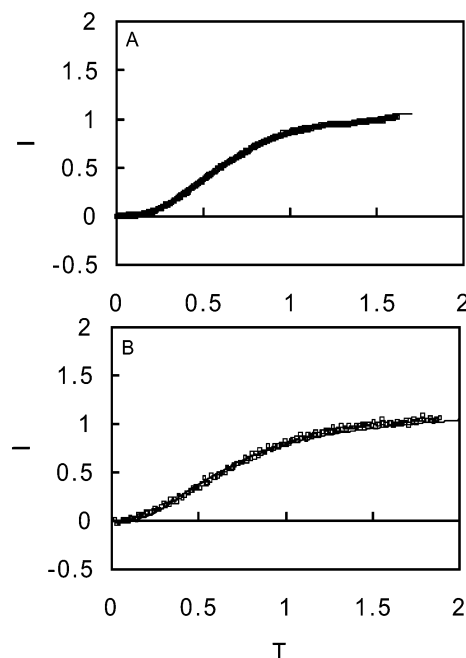
Figure 9. Experimental (symbols) and calculated (solid line) normalized current−time curves. (A) A tip voltage step of + 4.0 V. Fitting parameters for eq 1: $1/L = 0.6$, $I_{e,ss} = 0.99$, $\tau = 1.85$, the normalized ionic current, I_i, was negligibly small (≤0.005) as compared to the normalized electronic current, I_e, on a time scale of about 1 s.. (B) A tip voltage step of −3.0 V. Fitting parameters: $1/L = 0.6$, $I_{e,ss} = 0.93$, $\tau = 0.36$, $I_i ≤ 0.005$. Time scale, about 3 s. I and T are the normalized current and time, respectively.
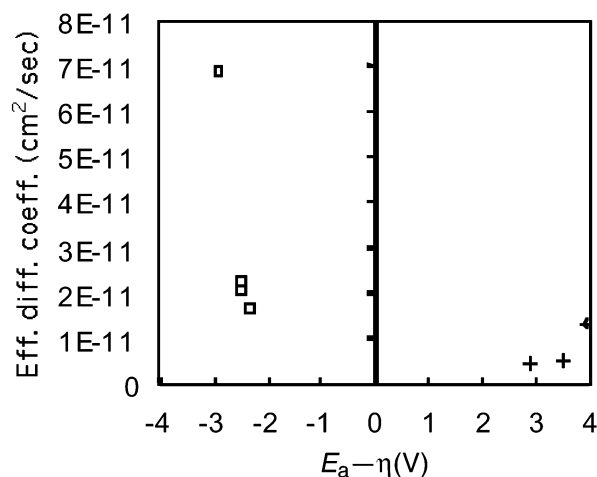
Figure 10. Effective diffusion coefficients of electron (squares) and holes (pluses) as functions of (applied voltage-overpotential at the tip), $(E_a - \eta)$.

transport and also light emission with short turn-on time. For a given bias, to increase the electric-field strength in the bulk of the film, one may also choose a proper pair of chemically and electrochemically stable electrodes to decrease the carrier injection barrier. It is also better to optimize bulk ionic conductivity, because ionic space charge relaxation will degrade the internal electric field in the long run.

Conclusions

Spin-cast $[Ru(bpy)_3(ClO_4)_2]$ thin films contain uniformly distributed nanostructures as imaged with a shear-force SPM combined with the ECL technique. These nanostructures produce heterogeneity in the current and luminescence responses of the films. Our results, in agreement with recent studies on
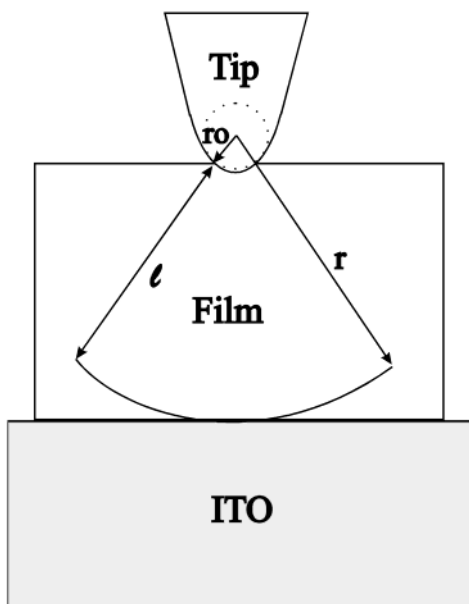
1786 *J. Phys. Chem. B, Vol. 107, No. 8, 2003*

Fan and Bard

Figure 11. Approximate representation of the tip and the substrate as two concentric spherical conductive segments.

related thin layer cells,[3] demonstrate that both single and double charge carrier (unipolar and bipolar) injection take place in these thin films, depending on the magnitude of the bias voltage. The potential-step transients allow the determination of the effective diffusion coefficients of charge carriers. We show that the effective diffusion coefficients of electrons and holes depend strongly on the electric-field strength (or the applied voltage).

Appendix

Model. We consider the case of low absolute tip bias ($|E_a|$ < 2.7 V) and single carrier injection. We assume a film of thickness, ϑ, on a conductive substrate with an initial uniform distribution of Ru(bpy)$_3^{2+}$ (concentration, C^*) and ClO$_4^-$ counterion (concentration, $2C^*$). For a negative tip bias after electron injection, some Ru(bpy)$_3^{2+}$ is reduced to Ru(bpy)$_3^+$ (which are equivalent to electrons in the film). At all times,

$$C_{Ox} + C_{Red} = C^* \tag{A1}$$

where Ox is the +2 state and Red is the +1 state (for hole injection at the tip, Ox is the +3 state and Red is the original +2 state). After injection, the conductivity is mainly due to electron hopping (negative tip bias) or hole hopping (positive tip bias). One approach is a calculation of the mobility of the electrons or holes based on solution of the Nernst−Planck equation that treats the effects of both diffusion and migration (drift) on carrier mobility. Simulations of this case, accounting for the variation of field with time, have been carried out for cells of this type[3b] or in solution with no or low supporting electrolyte.[12] The alternative approach used here treats this problem as diffusion in terms of a single diffusion equation and an effective diffusion coefficient, D_{eff}, that is a function of concentration and electric field strength (or applied potential).[10,11] We adapt this approach due to its simplicity and analytical accessibility for data extraction. For simplicity, we also approximate the tip and the substrate as two concentric spherical conductive segments (Figure 11). The diffusion problem for electron injection into a thin layer of redox material initially containing only oxidized electroactive moieties can then be formulated for the electrons (i.e., the reduced form of the redox material) as follows:

$$\partial C_{Red}/\partial t = D_{eff}\partial^2 C_{Red}/\partial r^2 + 2(D_{eff}/r)\,\partial C_{Red}/\partial r$$
$$t > 0, \quad r > r_0 \tag{A2}$$

$$C_{Red}(r,0) = 0; \quad C_{Ox}(r,0) = C^* \quad r > r_0 \tag{A3}$$

$$C_{Red} \text{ is finite for all } t \text{ and } r \tag{A4}$$

in which r_0 is the tip radius of curvature.

Assuming that the heterogeneous electron-transfer reaction (electron injection) at the tip is rapid, so that the Nernst relationship holds:

$$C_{Ox}{}^s/C_{Red}{}^s = \exp(nf\eta) = \theta \tag{A5}$$

where η ($= E_T - E^{\circ\prime}$) is the tip overpotential and E_T is the tip potential. $E^{\circ\prime}$ is the standard potential for the redox couple in the film, which is equivalent to the formal potential of a redox couple in solution, $f = F/RT$, F is the Faraday, R is the gas constant, T is the absolute temperature, and n is the number of electrons involved in the heterogeneous electron-transfer process ($=1$). $C_{Red}{}^s$ and $C_{Ox}{}^s$ are the concentrations of the reduced and oxidized moieties at the tip surface, respectively.

At the substrate (ITO)/film boundary, the electron flux is given by:

$$i_e/nFA = D_{eff}[\partial C_{Red}(r,t)/\partial r]_{r=\vartheta+r_o} \tag{A6}$$

where i_e is electronic diffusion current and A is the active surface area of the substrate.

One could also consider finite kinetics for electron transfer at the substrate/film interface as a boundary condition, but this is not discussed here. As a first approximation, we assume that the electric field in the bulk of the thin film (i.e., except at a Helmholtz layer at the surface of tip and substrate) is uniform and independent of time over the time scale of interest for the transient. This assumption is apparently justified, because this simplified model proved to be sufficiently accurate to provide a good quantitative fit between theory and experimental results, except for a high voltage step. Under such conditions, the solution of eqs A1−A5 gives $\bar{C}_{Red}$ (the Laplace transform of C_{Red}) at negative tip bias (after some mathematical manipulation)[9,11,13]

$$\bar{C}_{Red} = C^*/s - \{r_0\theta C^*/[r(1+\theta)s]\} \times$$
$$\exp[-(r - r_0)(s/D_{eff})^{1/2}] \tag{A7}$$

where

$$\bar{C}_{Red} = \int_0^\infty C_{Red}\,e^{-st}\,dt$$

Inverse Laplace transform of $\bar{C}_{Red}$ gives:

$$C_{Red} = C^* - \{\theta r_0 C^*/[(1+\theta)r]\}\,\text{erfc}((r - r_0)/2D_{eff}{}^{1/2}t) \tag{A8}$$

where erfc is the error function complement and θ is given by eq A5.

Solid-State Molecular Electroluminescent Devices

J. Phys. Chem. B, Vol. 107, No. 8, 2003 **1787**

Combination of eq A6 with eq A8 yields the expression for the diffusion current.

$$i_e = i_{e,ss}\{\text{erfc}[\vartheta/(2(D_{eff})^{1/2}t)] + [(\vartheta + r_0)/(\pi D_{eff})^{1/2}t] \times$$
$$\exp[-\vartheta^2/(4D_{eff}t)]\} \quad (A9)$$

where $i_{e,ss} = nF\Phi\pi D_{eff}r_0C^*(\theta/1 + \theta)$, in which Φ is the fractional area of the active spherical segment electrode.

In addition to the electronic current described above, there is an initial transient associated with the film resistance, R_B, and cell capacitance. The resistance of a thin film sandwiched between two concentric spherical-segment electrodes of inner radius, r_0, and outer radius, $r_0 + \vartheta$, can be expressed as:

$$R_B = (1/\Phi\pi\kappa)\{\vartheta/[r_0(r_0 + \vartheta)]\} \quad (A10)$$

where κ is the ionic conductivity of the film and is given by $F|z|uC$ (we assume no electronic conductivity in the film before charge injection), z is the charge of the anion, u is its mobility, and C is the concentration of mobile anions (we assume the cations are fixed). The capacitance of the cell is dominated by the double layer capacitance near the tip, c_T, which can be expressed as

$$c_T = \epsilon_o\epsilon\Phi\pi r_0^2/\lambda \quad (A11)$$

in which ϵ_o is the permittivity of free space, ϵ is the permittivity of the film, and λ is the effective thickness of the double layer near the tip. The ionic current transient can thus be approximated as

$$i_i = i_{i,0}\exp(-t/\tau_\Omega) \quad (A12)$$

Here $i_{i,0} = E_B/R_B = \Phi\pi\kappa r_0(r_0 + \vartheta)E_B/\vartheta$, E_B is the voltage drop across the bulk film, and τ_Ω is the ohmic or dielectric relaxation time, which is given by $R_Bc_T = \epsilon_o\epsilon r_0\vartheta/[\kappa\lambda(\vartheta + r_0)]$.

Combination of eq A9 with eq A12 yields the total normalized current, I, expressed as

$$I = I_{e,ss}[\text{erfc}(1/(T)^{1/2}) + \{2(1 + 1/L)/(\pi T)^{1/2}\}\exp(-1/T)] +$$
$$I_{i,0}\exp(-\tau T/\tau_\Omega) \quad (A13)$$

where $I = i/i_l = (i_e + i_i)/i_l$, $I_{e,ss} = i_{e,ss}/i_l$, $I_{i,0} = i_{i,0}/i_l$, $L = \vartheta/r_0$, $T = t/\tau$, $\tau = \vartheta^2/(4D_{eff})$, and i_l is the diffusion-limited current plateau, which is given by $nF\Phi\pi r_0 4D_{eff}C^*$. A similar equation can also be derived for the transport of holes.

This is a relatively simple approximate analytical equation, which can be used to fit the experimental current transients with reasonable accuracy as long as the carrier injection rate is not too high and the electric field across the bulk film does not deviate substantially from a constant. To our knowledge, a generalized treatment for carrier injection and transport in a point contact to a planar substrate configuration has not been solved analytically but can be addressed by numerical or digital simulation techniques as described in the literature.[3b,10b] Rigorous treatment of those current−time curves, as shown in Figures 5 and 6, with numerical or digital simulation techniques is interesting but not yet accomplished.

References and Notes

(1) (a) Sheats, J. R.; Antoniadis, H.; Hueschen, M.; Leonard, W.; Miller, J.; Moon, R.; Roitman, D., Stocking, A. *Science* **1996**, *273*, 884. (b) Berggren, M.; Inganas, O.; Gustafsson, G.; Rasmusson, J.; Andersson, M. R.; Hjertberg, T.; Wennerstrom, O. *Nature* **1994**, *372*, 444. (c) Greenham, N. C.; Moratti, S. C.; Bradley, D. C.; Friend, R. H.; Holmes, A. B. *Nature* **1993**, *365*, 628. (d) Gustafsson, G.; Cao, Y.; Treacy, G. M.; Klavetter, F.; Colaneri, N.; Heeger, A. J. *Nature* **1992**, *357*, 477.

(2) (a) Lyons, C. H.; Abbas, E. D.; Lee, J.-K.; Rubner, M. F. *J. Am. Chem. Soc.* **1998**, *120*, 12100. (b) Elliott, C. M.; Pichot, F.; Bloom, C. J.; Rider, L. S. *J. Am. Chem. Soc.* **1998**, *120*, 6781. (c) Wu, A.; Yoo, D.; Lee, J.-K.; Rubner, M. F. *J. Am. Chem. Soc.* **1999**, *121*, 4883. (d) Handy, E. S.; Pal, A. J.; Rubner, M. F. *J. Am. Chem. Soc.* **1999**, *121*, 3525. (f) Maness, K. M.; Masui, H.; Wightman, R. M.; Murray, R. W. *J. Am. Chem. Soc.* **1997**, *119*, 3987. (g) Maness, K. M.; Terrill, R. H.; Meyer, T. J.; Murray, R. W. *J. Am. Chem. Soc.* **1996**, *118*, 10609. (h) Rudmann, H.; Shimada, S.; Rubner, M. F. *J. Am. Chem. Soc.* **2002**, *124*, 4918.

(3) (a) Gao, F. G.; Bard, A. J. *J. Am. Chem. Soc.* **2000**, *122*, 7426. (b) Buda, M.; Kalyuzhny, G.; Bard, A. J. *J. Am. Chem. Soc.* **2002**, *124*, 6090. (c) Liu, C. Y.; Bard, A. J. *J. Am. Chem. Soc.* **2002**, *124*, 4190.

(4) McCord, P.; Bard, A. J. *J. Electroanal. Chem.* **1991**, *318*, 91.

(5) (a) Tokel-Takvoryan, N. E.; Hemingway, R. E.; Bard, A. J. *J. Am. Chem. Soc.* **1973**, *95*, 6582. (b) Luttmer, J. D.; Bard, A. J. *J. Phys. Chem.* **1981**, *85*, 1155. (c) Rubinstein, I.; Bard, A. J. *J. Am. Chem. Soc.* **1980**, *102*, 6641. (e) Itoh, K.; Honda, K. *Chem. Lett.* **1979**, 99.

(6) (a) Mirkin, M. V.; Fan, F.-R. F.; Bard, A. J. *Science* **1992**, *257*, 364. (b) Fan, F.-R. F.; Mirkin, M. V.; Bard, A. J. *J. Phys. Chem.* **1994**, *98*, 1475.

(7) Fan, F.-R. F.; Bard, A. J. *J. Electrochem. Soc.* **1989**, *136*, 3216.

(8) Karrai, K.; Grober, R. D. *Appl. Phys. Lett.* **1995**, *66*, 1842.

(9) Bard, A. J.; Faulkner, L. R. In *Electrochemical Methods: Fundamentals and Applications*, 2nd ed.; Wiley: New York, 2001.

(10) (a) Dahms, H. *J. Phys. Chem.* **1968**, *72*, 362. (b) Andrieux, C. P.; Saveant, J. M. *J. Phys. Chem.* **1988**, *92*, 6761.

(11) (a) Murray, R. W. In *Electroanalytical Chemistry*; Bard, A. J., Ed.; Marcel Dekker: New York, 1984; Vol. 13. (b) Ruff, I.; Botar, L. *Chem. Phys. Lett.* **1986**, *126*, 348. (c) Laviron, E. *J. Electroanal. Chem.* **1980**, *112*, 1. (d) Andrieux, C. P.; Saveant, J.-M. *J. Electroanal. Chem.* **1980**, *111*, 377. (e) Peerce, P. J.; Bard, A. J. *J. Electroanal. Chem.* **1980**, *114*, 89.

(12) See, for example: Smith, C. P.; White, H. S. *Anal. Chem.* **1993**, *65*, 3343.

(13) (a) Bateman, H. In *Tables of Integral Transforms*; McGraw-Hill: New York, 1954; Vol. 1. (b) Doetsch. G. In *Laplace Transformations*, Dover: New York, 1953.